Recurrent network dynamics reconciles visual motion segmentation and integration

N. V. Kartheek Medathati, James Rankin, Andrew I Meso, Pierre Kornprobst, Guillaume S Masson

Recurrent network dynamics reconciles visual motion segmentation and integration

N.V. Kartheek Medathati, James Rankin, Andrew I. Meso, Pierre Kornprobst, Guillaume S. Masson

RESEARCH REPORT
N° 9041
March 2017
Project-Team Biovision

ISSN 0249-6399 ISRN INRIA/RR--9041--FR+ENG

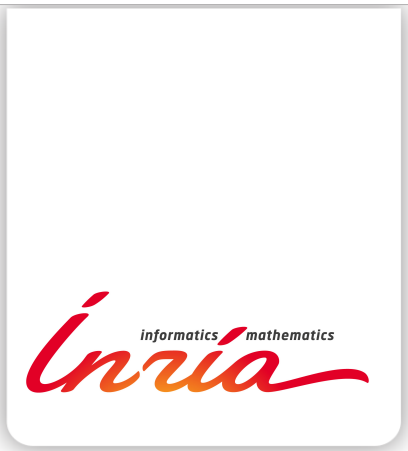

Recurrent network dynamics reconciles visual motion segmentation and integration

N.V. Kartheek Medathati*, James Rankin[†‡], Andrew I. Meso[§¶], Pierre Kornprobst*, Guillaume S. Masson[§]

Project-Team Biovision

Research Report n° 9041 — March 2017 — 24 pages

Abstract: In sensory systems, different computational rules are postulated to be implemented by different neuronal subpopulations, each one being characterised by a particular tuning function. For instance, in primate cortical area MT, different classes of direction-selective cells have been identified and related to either motion integration, segmentation or transparency. Still, how such different tuning properties are constructed is unclear. The dominant theoretical viewpoint postulates that differential weighting of MT inputs along the linear-nonlinear feedforward cascade is sufficient to build these different cell classes but it does not account for their complex temporal dynamics and their versatility when facing different input statistics. Here, we demonstrate that a recurrent network model of visual motion processing can reconcile these different properties. We show how excitatory and inhibitory recurrent connections, within a direction representation space, shape neuronal motion direction tuning and implement different computational rules such as vector averaging, winner-take-all or superposition. The model also captures ordered temporal transitions between these behaviours. In particular, depending on the inhibition regime the ring network can switch from motion integration to motion segmentation, thus being able to compute either a single pattern motion or to superpose multiple inputs as in motion transparency. We thus demonstrate that recurrent architectures can adaptively give rise to different cortical computational regimes depending upon the input statistics, thus reconciling the two facets of sensory processing: integration and segmentation.

Key-words: Visual motion integration, dynamical systems, direction selectivity, ring model

* Université Côte d'Azur, Inria, Biovision team, France
† Department of Mathematics, University of Exeter, UK
‡ Center for Neural Science, New York University, USA
§ Institut de Neurosciences de la Timone, CNRS and Aix-Marseille Université, France
¶ Psychology, Faculty of Science and Technology, Bournemouth University, UK

RESEARCH CENTRE
SOPHIA ANTIPOLIS – MÉDITERRANÉE

2004 route des Lucioles - BP 93
06902 Sophia Antipolis Cedex

La dynamique récurrente de réseaux permet de réconcilier la segmentation et l'intégration du mouvement visuel

Résumé : Dans les systèmes sensoriels, différentes règles computationnelles sont supposées être implémentées par différentes sous-populations neuronales, chacune étant caractérisée par une fonction de sélectivité. Par exemple, dans la zone corticale des primates MT, différentes classes de cellules sélectives à la direction ont été identifiées et liées à l'intégration du mouvement, à la segmentation ou à la transparence. Cependant, la façon dont ces fonction de sélectivité sont construites n'est pas claire. Le point de vue théorique dominant postule que la pondération différentielle des entrées de MT le long de la cascade montante linéaire non linéaire est suffisante pour construire ces différentes classes de cellules, mais ne tient pas compte de leur dynamique temporelle complexe et leur versatilité face à différentes statistiques d'entrée. Ici, nous démontrons qu'un modèle de réseau récurrent de traitement du mouvement visuel peut reconcilier ces différentes propriétés. Nous montrons comment les connexions récurrentes excitatrices et inhibitrices, au sein d'un espace de représentation de direction, forment la selectivité neuronale à la direction du mouvement et implémentent des règles de calcul différentes telles que la moyenne des vecteurs, le "tout au vainqueur" (*winner-take-all*) ou la superposition. Le modèle capture également les transitions temporelles ordonnées entre ces comportements. En particulier, en fonction du régime d'inhibition, le réseau en anneau (*ring model*) peut passer d'une intégration de mouvement à une segmentation de mouvement, ce qui permet de calculer soit un seul mouvement de motif, soit de superposer des entrées multiples comme dans les mouvements transparents. Nous démontrons ainsi que les architectures récurrentes peuvent adapter de façon adaptative des régimes de calculs corticaux différents en fonction des statistiques d'entrée, afin de reconcilier les deux facettes du traitement sensoriel: l'intégration et la segmentation.

Mots-clés : Intégration du mouvement, systèmes dynamiques, selectivité à l'orientation, *ring model*

Introduction

Sensory inflows received by animals are highly complex and ambiguous with multiple local sensory events occurring simultaneously. A challenging computational task faced then by any sensory system is to either integrate or segment these local signals in order to encode behaviourally-relevant information. This is well illustrated by visual motion processing. Local motion signals must be selectively integrated in order to extract and reconstruct the direction and speed of a particular surface [4]. But the same set of local signals must also be kept segregated from the many others belonging to distinct surfaces that can be either adjacent (e.g., motion boundaries) or overlapping (e.g., motion transparency). The rules governing motion integration and segmentation have been extensively investigated at both perceptual and physiological levels (see [5, 10, 3] for reviews). For instance, when presented with two motion directions, the primate visual motion system can group them according to linear (i.e., vector average) or nonlinear (i.e., intersection-of-constraints) rules [1, 26]. It can also segment them by either suppressing one of the two inputs (i.e., winner-take-all) or simultaneously representing both of them (i.e. superposition) as in the challenging case of motion transparency [45, 35, 47].

In the macaque middle-temporal (MT) cortical area, a pivotal processing stage for object motion computation [3], different classes of direction-selective neurons have been linked to each of the aforementioned computational rules (e.g. [26, 35, 47, 50, 21]). When presented with moving plaids made of two superimposed sinusoidal gratings drifting in different directions, some cells encode only one of the two components (i.e. component cells) while others encode the pattern motion direction after combining them (i.e. pattern cells) [26, 40]. Recently, Xiao and Huang [50] investigated the responses properties of MT cells when tested with bi-directional random dot patterns. A majority of MT cells exhibit a single peak tuned to either one of the components or to their mean direction, implementing winner-take-all or vector average computations, respectively. Other cells show two peaks and could thus represent two overlapping motion directions [50]. At the population level, a similar set of canonical tuning curves were reported and ascribed to either motion integration, motion segmentation or motion transparency, respectively [40, 45, 50].

Several modelling studies have suggested that these subpopulations span a continuum along which their feedforward, direction-selective inputs from area V1 are differently weighted [43, 41, 50]. There are however several pitfalls with linear-nonlinear (LN) feedforward models. First, their static nonlinearities cannot render the complex temporal dynamics of these tuning functions that were shown to shift over time from, say vector average to either winner-take-all or transparency solutions [28, 44, 50, 47]. Second, they cannot explain why exchanging plaid patterns by random-dot patterns with similar motion component directions scrambles the cell's classification, nor can they explain contradictory results reported when attempting to predict MT cell tuning to one stimulus from the other [50, 21]. An alternative approach would be considering sensory integration and segmentation as threads of a complex dynamical computation where inhibition and excitation are shaped adaptively to the spatiotemporal properties of the inputs [7]. Only a handful of computational studies have applied this theoretical framework to visual motion processing. They succeed in explaining some properties of MT neuronal tuning functions, but have so far focused on only a small subsample of tuning classes and motion inputs [48, 9, 51, 32, 16, 36]. We designed a neural field dynamical model working in a motion direction space and investigated the interplay between its connectivity and input properties. We show that the different MT neuronal classes reported previously are steady-state solutions of the dynamical system, their strength and stability varying with both input statistics and excitation-inhibition balance. In specific parameter regions, the network exhibits coexisting states, leading to multi-stability across trials without plasticity rules. We show how slightly asymmetric inputs can stabilise the network behaviour. The temporal dynamics of direction tuning and the

transitions between different network states when varying input statistics are also well captured. These results demonstrate a fundamental role for recurrent connections in shaping basic cortical computations and show that sensory neural circuits can dynamically switch from integration to segmentation depending on input statistics.

Results

We studied the behaviour of a voltage-based network model that describes the local mean field potential (see Methods and SI Methods) of a population of directionally tuned MT neurons under different inputs and excitation-inhibition interactions. We focused on the properties of the steady state solutions such as the shape of the direction tuning functions, their number of peaks at convergence and the peak positions with respect to the driving inputs. A recent and comprehensive physiological study of MT responses to different types of uni- or bi-directional motion stimuli [50] provides an ideal point of comparison for our model simulations.

The network represents a sub-population of N directionally tuned MT neurons with a smoothly varying directional preference, represented by an angle θ (Fig. 1a). Each cell receives afferent inputs from a V1 layer, where stimuli are encoded by Gaussian distributions for each motion input (Fig. 1b). The input is defined by the peak width of each Gaussian distribution (PW) and the peak separation between the two Gaussian distribution (PS) to simulate different types of bidirectional motion stimuli. Distributions are broader for gratings than for random dot patterns, reflecting both the larger ambiguity in the grating motion direction and the properties of V1 and MT cells [34, 33]. MT neurons also receive inputs from the local recurrent interactions (Fig. 1c). This local recurrent connectivity depends only on the directional difference, being locally excitatory and laterally inhibitory. It implements a typical centre-surround connectivity kernel defined by a weighted difference between Excitation and Inhibition Gaussians distributions in the motion direction space. Note that we consider the limiting case of global lateral inhibition (very broad inhibition Gaussian) and so preserve higher order harmonics rather than reducing to a two [12] or three modes approximation [8, 37]. The connectivity kernel is defined by only two parameters: the extent in direction space of lateral excitation (α) and the strength of inhibition (β) (Fig 1c).

Network behaviour

Using numerical bifurcation analysis, we first identified the stable solutions and the parameter regimes over which these different solutions coexist. When the network is stimulated with a bidirectional input, varying PS leads to different types of solutions. These are shown in a bifurcation diagram in Fig. 1d, where solid and dashed curves represent stable and unstable solution branches, respectively. The tuning curves of the three stable solutions are illustrated in the right-hand panels and corresponded to the three main neuronal tuning reported by [50]. Cases **a,b** and **c** in Fig. 1d correspond to the observed vector average (VA), winner-take-all (WTA) and transparency (T) tuning functions, respectively. For small PS, VA is the only possible solution. For large PS, WTA and T coexist. For an intermediate range ($95 \lesssim PS \lesssim 130$), we identify a critical operating regime where the model is capable of producing the three prototypical tuning functions within the same parameter region. We observed that the WTA solution was side-biased (SB), indicating that the other, competing input was not fully suppressed, similar to the empirical evidence reported in macaque area MT [50]. Unstable solution branches **d,e** can link the stable branches, but are not critical in this study. Stable solution branches terminate at bifurcations points where a qualitative change in model behavior occurs. We note that the intersection of **a,d** is a pitchfork bifurcation (with two complementary WTA branches overlapping

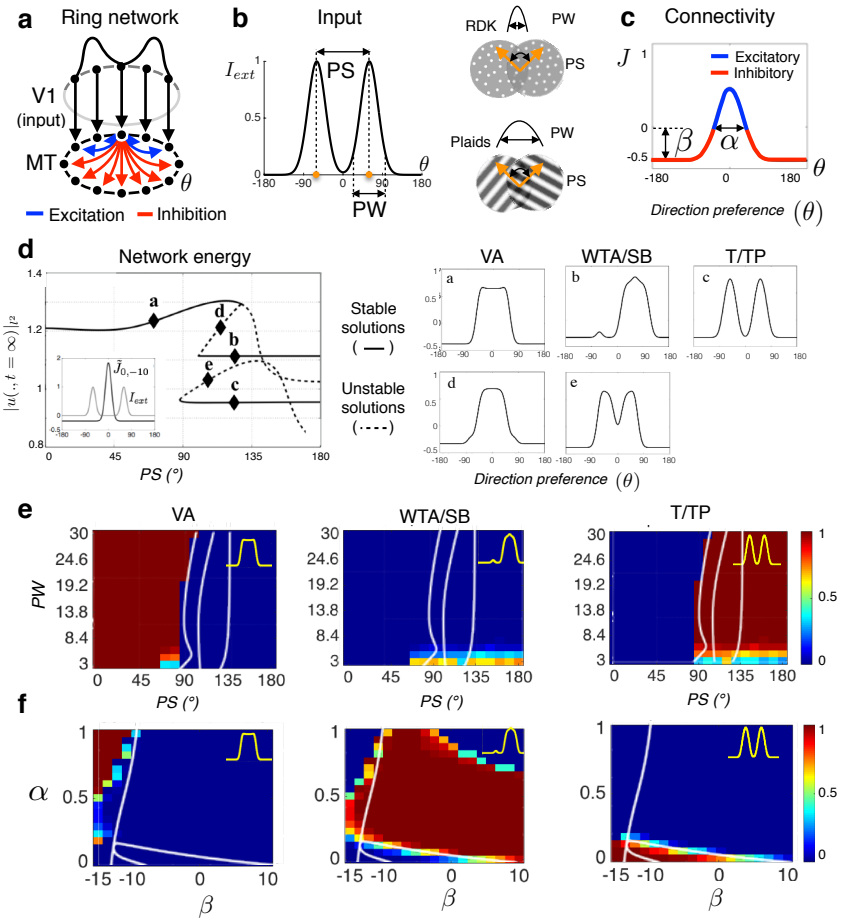

Figure 1: Ring model behaviour and likelihood of convergence. **(a)** Illustration of a ring network modelling visual motion integration at MT cells level, with V1 input and recurrent connections. **(b)** MT inputs are defined as two Gaussian distributions parametrised by PS and PW, corresponding to different random dot and plaid patterns. **(c)** The centre-surround connectivity kernel in motion direction space is parametrised by α and β, defining a family of kernels. **(d)** Network energy is computed from the I2-norm of the steady-state solution. The bifurcation diagram is plotted as a function of parameter PS (with PW=10, $\alpha = 0$, $\beta = -10$ being fixed) to illustrate both stable (a,b,c) and unstable solutions (d,e) for each branch and their corresponding direction tuning functions. Three classes of solutions co-exist: vector average (VA), winner-take-all (WTA) and transparency (T). Note that referring to [50], winner-take-all will also be designated as side-biased (SB) and transparency as two-peaked (TP) tuning curves. **(e)**, **(f)** show attractor strength of each steady-state solutions (a,b,c), measured as a probability of reaching it from repeated simulations with randomised 100 initial conditions, and varying either input parameters (with fixed $\alpha = 0$ and $\beta = -10$) or connectivity parameters (with fixed PS=120 and PW=10), respectively.

in the projection shown) while intersections of **d,b** and **c,e** are fold bifurcations. [19]. Two unstable branches overlap in this projection at PS≈145 but are not connected. These can be tracked in terms of a two parameters phase diagram, delineating entire parameter regions where different types of solutions exist (see continuous white lines in (Fig. 1e,f).

The network behaviour is best characterised by maps of attractor strength unveiling which of the stable solutions identified in the bifurcation analysis dominates. Attractor strength of each solution, measured as a probability of reaching it from 100 repeated simulations with randomised initial conditions, was computed at every combination of both external (input: PS,PW) and internal (connectivity kernel: α, β) parameters (colour maps in Fig. 1e,f). Although in a given parameter regime, two or more direction tuning shapes can coexist as stable solutions, the network might be much more likely to converge to one of these from a random initialisation. In Fig 1e, the likelihood of the VA solution was maximal for small PS, regardless of the PW (see left panel). For large PS, the transparency case dominates over a large range of PW (see right panel). For narrow (small PW) and widely (large PS) separated peaks the WTA solution occurs in roughly 60 % of trials and TP otherwise (see middle panel). In Fig 1f, we observe that maintaining two peaks at population level requires both low inhibition and narrow excitation (small β and α, see right panel) whereas VA requires low inhibition but broad excitation (small β and large α, see left panel) . The WTA solution is highly probable across a wide range of inhibition strength and excitation extent. Thus, the emergence of different network states corresponding to either motion integration or segmentation results from the interplay between the properties of the inputs and the shape of the centre-surround interactions in direction space. We propose that different properties of lateral connections is part of what distinguishes observed cell classes. In the following sections, we investigate the dynamics of these cell classes, focusing successively on the relationships between single-cell and population tuning, the stability of direction tuning and its temporal dynamics and the shift from one solution to another as a function of input statistics.

Local recurrent interactions lead to prototypical tuning behaviours found in macaque area MT

In macaque area MT, Xiao and Huang [50] extensively documented the single-unit responses to random dot patterns made of either one or two motion direction components. For single motion inputs, direction tuning ressembles the classical Gaussian-like functions as shown in panel a0 in Fig. 2a. Using overlapping motion inputs with different degrees of component separation, they reported a handful of prototypical behaviours illustrated in Fig. 2a. For a fixed PW and two direction differences (PS), they described three different classes of cells. Type a1 (PS=45°) represents the vector average (VA) of the two motion inputs while a3 (PS=135°) superposes them, yielding to a two peaked tuning function (TP). Type a2 (PS=120°) and its mirror symmetric (not shown) form a single class where one or the other of the two inputs is suppressed. These side-biased (SB) cells implement a weak winner-take-all where an influence from the suppressed inputs can still be seen. Here we show that a population of direction selective cells can produce these prototypical behaviours through the influence of local recurrent interactions.

We simulated the network with a set of input pattern directions (see Methods). Figure 2b illustrates the MT population direction preference, as a function of the average input motion direction. Four cases are illustrated, corresponding to different recurrent connectivity regimes (row c, Fig. 2) and to different input parameters (PW and PS given in **(b)** and plotted as orange curves in row **(d)**, Fig. 2). Sampling the population vertically gives the MT population tuning (plotted in row **(d)**) and sampling horizontally gives the single cell tuning (plotted in **(e)**). Column b0 shows that the network accurately represents the unidirectional input. Column b3 illustrates the population and single cell tuning for two widely separated inputs (120°) and

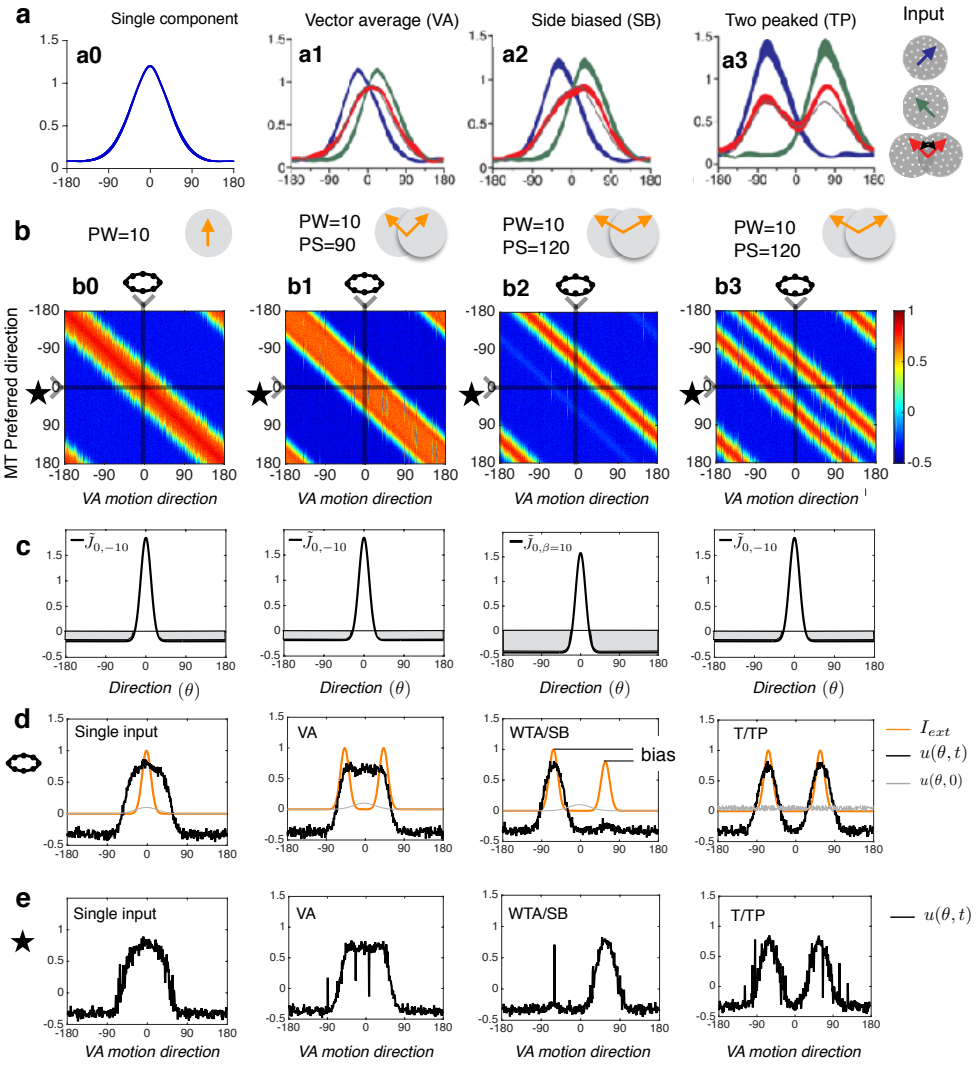

Figure 2: Recurrent interactions lead to prototypical tuning behaviours found in MT. **(a)** Four examples of prototypical single cell tuning functions found in macaque area MT (adapted from [50]). Blue and green curves show the tuning functions obtained when presented with a dot pattern moving coherently in one of the two directions. Red curves show the tuning functions obtained when the two direction components overlapped, forming a bidirectional moving pattern. For comparison, the thin blue curves are the predicted vector average profile from the single input tuning functions. **(b)** We simulated the ring network by sequentially varying the pattern direction of the driving input for a uni-directional stimulus (column b0) or different bi-directional patterns (columns b1-b3). The connectivity kernels used for each set of simulation are indicated in **(c)**. The orange curves show the network inputs. **(d)** The tuning function of the MT population (indicated by a ring) can be obtained by cutting a vertical slice in plot b. Conversely, a single-cell tuning (indicated by a star) is obtained from an horizontal slice and shown in **(e)** Notice that for column b2, single-cell and population tuning are symmetrical as we conserve the same sampling direction across all b0-b3 conditions.

the same recurrent connectivity, with a low inhibition regime ($\beta = -10$). The two peaks are preserved, yielding to a bimodal tuning function (T/TP). Notice that each peak is now sharper than observed with a single direction input, thanks to recurrent inhibition. Narrowing the input direction difference to 90° (column b1) changed the tuning functions at both population and single-cell levels: now the vector average (VA) is represented. Using the same input as in b3, column b2 illustrates that the network shifted to a winner-take-all solution when inhibition strength was increased ($\beta = 10$). Notice that, to favour the existence of a small second peak, we introduced a small input bias in favour of the $-60°$ direction (Fig. 2d, column b3, orange curve) because a high inhibition regime together with a small bias within the input strengths leads to a robust side-biased (WTA/SB) behaviour. Indeed, a small response to the suppressed direction is still evident, due to the local recurrent excitation, in both the population and single-unit tunings. We will further compare symmetric and asymmetric inputs later (see Fig. 3). Overall, by comparing biological (a0-a4) and simulated (b0-b4) responses one clearly see that the ring model can reproduce the three prototypical tuning functions observed in macaque area MT (e.g. [50, 21]. Note that model single cell selectivities can exhibit variability due to recurrent interactions. This can happen when the network is operating in a parameter regime where different solutions co-exist with one attractor largely (but not totally) dominating. In this case, input noise in the input can drive the network to different stable solutions from one simulation to the next due to the coexisting states shown in Fig. 1d. We will further investigate this below.

Fluctuations in component selection and population tuning reliability

One of the hallmarks of recurrent interactions is the existence of multiple stable solutions for the same set of parameters. Under such multi-stability, the network could converge to different stable states (with different direction tuning) from one trial to the next. This is evident from the bifurcation diagram shown in Fig. 1d where different solutions can coexist for a given input (e.g., see at PS=120°). Moreover, in the WTA regime, the network could select either of the two motion components when stimulated with inputs having purely symmetric component strength. Still, a stable tuning behaviour could emerge in regimes where only one of the tuning behaviours is dominant, due to either inhibition strength or the structure of the driving input. To probe network stability, we fixed the recurrent connectivity parameters and used random dot patterns (PW=20°) with a constant PS (120°) while varying the relative strength between the two motion components from 0.7 to 1 (Fig. 3, left-to-right columns). In empirical studies, the strength of one component could be reduced by decreasing its signal-to-noise ratio. For each condition, we ran 400 trials by sequentially shifting the vector average motion direction from 0 to 360°. The MT preferred direction is plotted as a colour map similar to Fig. 2b. Under these conditions, WTA solutions dominate the network dynamics when the two inputs have different strength (**(a-c)**). The lower row shows stable tuning function for both the population activity (red curves, lower row) and the sampled single-unit activity (black curve). The population activity matches the direction of the stronger input. When increasing the relative input strength to 0.9 (case **(c)**), the population response shifted from a pure WTA to a SB tuning function (see small bump at 60° for red curve in **(c)**, lower row). Now, single unit activities exhibited large fluctuations across directions, the sampled cell representing either one peak (i.e. SB tuning) or two peaks (i.e. T/TP tuning), with a strong dominance for the former. Hence, under this low inhibition regime ($\alpha = 0$, $\beta = -10$), the effective inputs must be slightly asymmetrical to produce the SB solution. With symmetric inputs (**(d)**), the two inputs yields to a shift in both population and single-unit tuning, now largely representing the two inputs (TP tuning) but with some occurence of the WTA solution. Note that the single-unit activity was now largely fluctuating across the different VA motion directions (**(d)** bottom row, black curve). As a consequence, with symmetrical inputs the

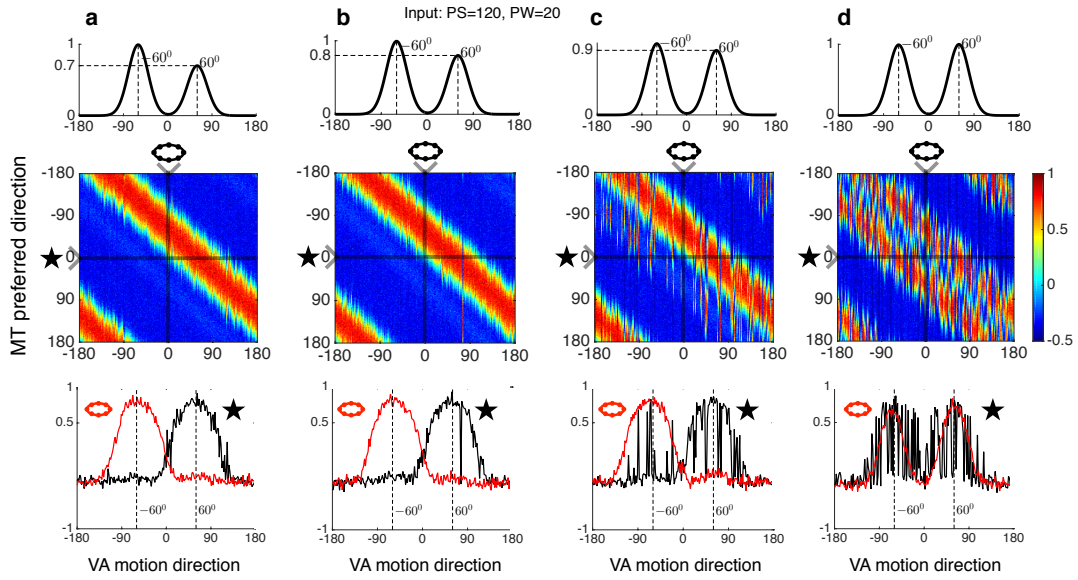

Figure 3: Tuning behaviour changes with respect to the asymmetry in the input. We simulated the network with a single set of driving input directions (PS=120°, PW=20°) and recurrent inhibition parameters ($\alpha = 0$, $\beta = -10$). From left to right-hand plots, the relative strength between the two inputs increases from 0.7 to 1. Upper row illustrates the network inputs. Middle row shows the model responses as a function of both VA motion direction and population preferred direction. Again, a vertical sampling of the response map gives the population tuning (ring) while an horizontal sampling (star symbol) provides the single-cell tuning. Population (red curve) and single-cell (black curves) tuning functions are then plotted against VA direction in the lower row.

ensemble of single-unit activities was much less consistent when the TP behaviour was observed at the population level (compare left- and right-hand columns in Fig. 3). We conducted the same analysis for other PS and PW values and obtained similar results: population tuning properties changed and were less consistent when inputs were strictly symmetrical.

Temporal dynamics

Several empirical studies have shown that MT neuronal selectivities gradually develop over time with a latency of 50-70ms [28, 44, 50]. Such temporal dynamics is well illustrated in the four examples taken from Xiao and Huang [50] and replotted in Fig. 4 for different PS values. The examples in panels **a,c** and **d** show that steady-state WTA/SB tuning functions can gradually emerge from different early tuning shapes such as VA (**a**), SB (**c**) or TP (**d**). In **b**, this particular cell first encodes the vector average direction (VA) of a random dot pattern with a (60°) direction difference. The response tuning then gradually evolves towards the steady-state T/TP attractor solution in our model, where the two inputs are superimposed. By comparing these response patterns with the linear prediction from neuronal responses to each of the two component presented alone, the authors [50] suggested that VA motion direction was suppressed while component mo-

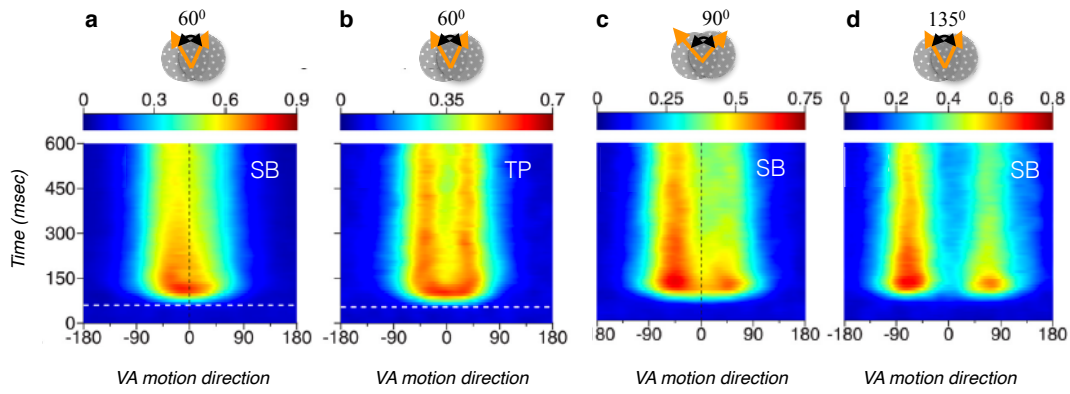

Figure 4: Four examples of temporal evolution of MT tuning functions.(**a-d**) show the temporal development of the subpopulation-averaged response tuning to bidirectional stimuli with different PS values [50]. (**a**) The initial response tuning peaks around the VA direction before gradually shifting to one single peak aligned with the population preferred direction, corresponding to the WTA solution. (**b**) For the same PS (60°), the two component motion directions gradually emerge, together with a strong suppression of the VA direction. (**c**) With PS=90°, the initial response is a broad tuning centred around the VA direction, before shifting towards the component motion aligned with the preferred-direction. (**d**) With larger PS (135°), the initial response tuning show two peaks (TP) before one peak is suppressed, leading to the SB tuning described above. All examples are adapted from Figures 6 and 8 of [50], respectively.

tions were facilitated. This observation is consistent with the widespread hypothesis that lateral excitatory interactions without inhibition could lead to early integration with a broadly tuned response. Later on, neuronal response could be further shaped by growing inhibition until they reach a stable solution that depends on the input statistics (e.g. [50, 47, 42]).

We tested this hypothesis by allowing inhibition strength (β) to evolve temporally with a slow time constant (100ms). Fig. 5 illustrates the model parameters and outputs for two instances of the temporal evolutions which were shown in Fig. 4**a** and **d**. The left-hand column corresponds to the VA-WTA transition. The right-hand column illustrates the time course of the TP-SB transition. Model and MT population (shaded box, from [50]) tuning dynamics are illustrated as both full time plots and a selection of time slices for comparison. Notice that the pure feedforward latency delaying the MT response by about 50ms was not simulated in the model dynamics. Upper panels show the time course of surround inhibition together with 3 time-lapses of the excitation/inhibition balance within the direction domain. The gradual increase of inhibition strength captures the temporal dynamics of MT motion direction processing. The left-hand panels show that the model population first encodes the VA solution. Slowly increasing inhibition shifts the tuning towards a WTA stable solution, together with an increased precision in the direction tuning, nicely simulating the biological data. The left-hand columns illustrates another temporal development when PS=135°. The initial response superimposes the two inputs, corresponding to the T/TP cases. Over time, one of the two peaks is suppressed while the other is enhanced. Notice that the former is not entirely suppressed such that until 300ms, the solution corresponds to the SB case. Later on, it entirely disappears and the late solution becomes a complete WTA tuning function, albeit with a broader tuning that was not reported

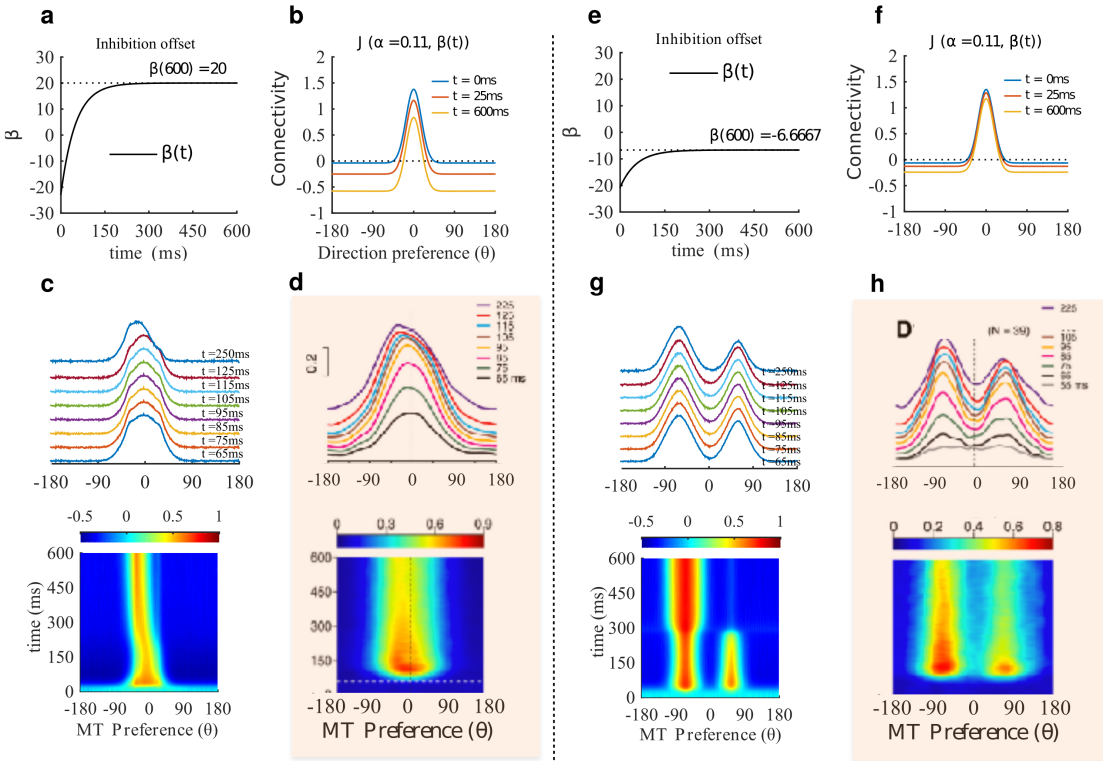

Figure 5: Temporal tuning behaviour. (**a-d**) Temporal development of the WTA solution. **(a)** Time course of inhibition, leading to different excitation/inhibition balance levels as illustrated at three different time lapses **(b)**. **(c)** Temporal evolution of population tuning in response to bidirectional stimuli with PS=60°. The model population responses is initially aligned with the VA direction, before slowly drifting to one of the component direction. The other motion direction is strongly suppressed, corresponding to the WTA solution illustrated by the direction tuning at different time lapses. The model dynamics renders the temporal evolution of an MT subpopulation as illustrated in **(d)**. (**e-g**) Temporal development from the TP to the SB solutions. Same plots as in the left-hand column. Biological data are taken from **(author?)** [50].

in the biological data. Furthermore, the two peaks are also shifted away one from another, corresponding to the development of motion repulsion [20] as noted in [50]. Again, the model dynamics capture the main characteristics of the TP/SB transition illustrated by the mean population activity reproduced in the shaded box.

Interestingly, our model could not replicate the transition from a broad VA towards a two peak (T/TP) response that was reported by [50] (see panel (**b**) in Fig. 4). There are two potential reasons for this limitation. First, the likelihood of the two peak solution is very small when the driving inputs are close and sharp (i.e. small PW) as in the case of random dot patterns. Therefore, most of the simulated temporal developments under these conditions occurred between VA and WTA solutions. Even when inhibition strength was set to favour the two-peaks steady-state solution, a large amount of noise was necessary to destabilise the early VA solution and reach the T/TP solution branch. Second, when the two motion components are close (PS=60°), Xiao and Huang reported that activity shifts from VA to WTA (Fig.4a) but for larger PS (90°

and 135°) activity spreads such that one component builds on while the other vanishes. Instead, under these conditions, the dynamics of our model is characterised by a steady activity of both components, failing to eliminate the weakest peak.

Predicting tuning behaviour for different types of bidirectional motion inputs

One remarkable property of pattern motion integration in macaque area MT is that cell responses to bidirectional plaid patterns cannot be fully predicted from bidirectional random dot patterns, and reciprocally [50, 21]. That is to say, a pattern cell identified with plaid patterns would not necessarily encode the vector average motion direction of a bidirectional random dot pattern. Xiao and Huang [50] systematically tested a large population of MT cells with both stimuli, across different PS values. From their data (see Table 2 in ref. [50]), we computed a migration plot illustrating the likelihoods of transition between cell types from one stimulus to another (Fig. 6.a). Note that when PS=135° for both plaids and random-dots patterns, the only difference in the input statistics for our model would be PW (i.e. the variance in each of the component motion direction provided by the V1 layer). Notice also that in biological studies, unclassified cells are defined only from the component/pattern correlation metrics and this class is not relevant for our model. Overall, the observed MT migration diagrams show that no strict migration rules were observed but there was rather small biases in how cell tuning migrates when comparing random dots and plaids. Xiao and Huang [50] observed a trend that VA and WTA cells observed with random dots at PS=60° were more likely to classified as pattern and component cells, respectively when tested with a plaid of PS=60°. When comparing random-dots and plaid patterns with similar PS (135°), T/TP and WTA cells predominantly were classified as pattern selective. Again, notice that a large fractions of cells that can be classified as either VA, WTA or TP cells in response to random dots were unclassified when tested with plaids, regardless of PS.

In our model, we can simulate these migration probabilities by examining the attractor strength of the stable solutions across variety of internal parameters allowing us to visualise how the attractor strengths would shift from one condition to another as illustrated in Fig. 6. To do so, we first measured the attractor strength of each solution in different connectivity regimes from 100 responses to a given input. From these, we constructed a likelihood map for this particular condition. Once the likelihood maps for all the solution types across the different inputs were obtained, we identified the connectivity regimes which could support transitions in one type of tuning for a particular input to other types of tuning with a different input by overlaying the thresholded maps (see the Methods section) in order to compute an overlap value that illustrate the relative likelihood of a particular migration, as illustrated in Fig. 6.c.

When fixing the model internal parameters (i.e. the excitation and inhibition balance) some migrations are more probable than others. With a random dot pattern of small PS (60°), VA and WTA/SB are the most probable states. When presented with a grating of large PS (135°), most VA responses become WTA/SB while WTA/SB responses remains largely identical. When grouping the model response tuning types within the pattern/component classification used for MT neurons with plaids, most of the WTA/SB and VA responses become component selective. Under a fixed inhibition regime, transitions towards pattern selectivity are very sparse. When equating PS between plaids and gratings (135°) as in [50], the migration patterns become even more dispersed, underlying the critical role of the relative width of motion inputs between the two stimulus types. The majority of WTA/SB responses remained but a significant fraction shifted towards the T/TP states. Only a small fraction of WTA/SB and T/TP responses migrated to VA, as the likelihood of representing pattern motion direction becomes very weak under such

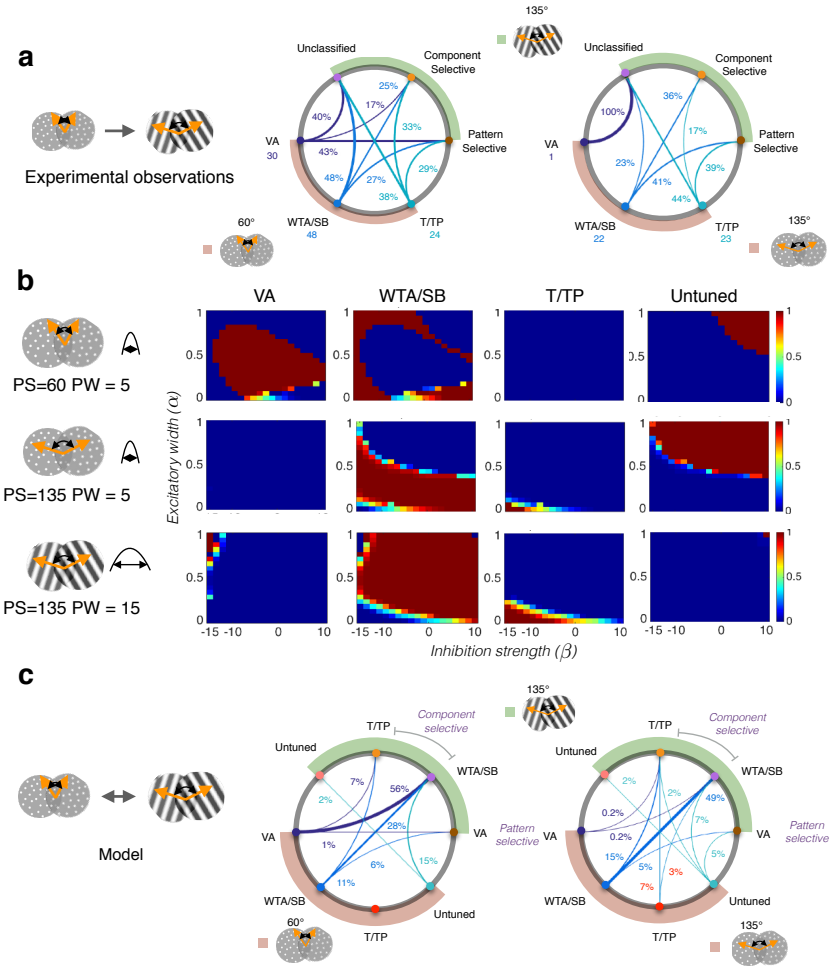

Figure 6: Responses properties change with input statistics. (**a**) Direction tuning properties of MT subpopulation shift when presented with either a bidirectional random dot pattern (RDS) or a moving plaid. Migration diagrams have been recomputed from the dataset of [50]. For each type of cell obtained with an RDS of PS either 60° or 135°, the diagram plots their probability of becoming either a pattern, a component or an unclassified cell when tested with a plaid pattern of PS=135°. Overall, the behaviour of a subpopulation cannot be predicted when migrating from one stimulus class to another. **b** Probability maps of each stable solution (VA, WTA/SB, T/TP, untuned) of the ring model with the same set of bidirectional stimuli, as a function of excitation width and inhibition strength parameters. **c** Migration diagrams of the ring model under the same conditions as in (a). The probability of migration from one regime to another is computed from the intersect between pairs of probability maps (see Methods and 7).For the sake of comparaison with (a), WTA/SB and T/TP responses to plaids can be regrouped as component selective responses, while VA states can be equated to pattern motion selectivity.

large PS.

Interestingly, some of the experimentally observed transitions could not be explained by changes in the driving input alone. For instance, the migration from T/TP to VA reported in both experiments by [50] (see Fig. 6.a) were never observed under fixed recurrent connectivity. Broadening excitation and strengthening inhibition are both necessary to enable these migrations. Moreover, maintaining the VA states across stimulus types would require to shift the excitation/inhibition balance. The somewhat arbitrary grouping of T/TP and WTA/SB states within the classical component selective types of MT neurons (and equating the VA and component selectivities) is somewhat arbitrary. This, together with the limitation that unclassified cell subpopulation was not specifically modelled, prevented us from fitting our model migration patterns to those observed in the neurophysiological studies. Nevertheless, future work with such a ring model could investigate how excitation/inhibition connectivity rules should adaptively change to better predict neuronal tuning changes with input statistics.

Discussion

A ring-model [2, 12] with a feature space of motion direction was used to investigate the tuning properties of MT cells in response to inputs with multiple motion directions. We systematically compared our model responses to a recent comprehensive description of MT direction selectivities under a large set of motion inputs [50]. Our simple dynamical model featuring recurrent interactions within MT can produce a surprisingly diverse set of network states that closely match the direction tuning functions associated with different subpopulations in macaque area MT. We qualitatively compared our model behaviour with one recent, comprehensive neurophysiological study [50]. These tuning functions correspond to the vector averaging (VA), winner-take-all (WTA and its variant, side-bias, SB) or superposition (two-peaks, TP) solutions to the visual motion integration/segmentation computations performed by these neuronal populations (see [26, 4, 3] for reviews). The model shows that these different tuning functions emerge from a single, adaptive recurrent network where excitation and inhibition can be tuned depending upon on input statistics. Moreover, these recurrent interactions give rise to co-existing network states, that can explain multi-stability and single-unit variability. Recurrent interactions can also explain the dynamics of these tuning functions, i.e. how they transition over time from one type of tuning to another tuning function, and how these subpopulations change behaviour when varying the statistical properties of the inputs. Therefore, the model reconciles a large bulk of recent empirical observations on the properties of area MT neurons, a key area for visual motion processing (e.g., see refs. [47, 50, 21]).

Recurrent interactions allow multiple behaviours from the same network

In our model, individual motion components (e.g., the individual gratings in a motion plaid or, a single dot-field with coherent direction in RDK) were represented by a Gaussian bump in the motion direction space. Inputs with multiple directions were captured by a combination of Gaussian bumps. Varying width and separation of these bumps allows for commonly studied component motion stimuli to be represented in the model. Recurrent connections in the motion-direction space were minimally parametrised by the width of excitation and strength of inhibition. Different network states were characterised in a systematic parameter study varying input statistics and internal connectivity parameters. We have shown that a variety of tuning behaviours observed in the sub-populations of macaque direction selective MT neurons could be explained by a recurrently interacting group of cells tuned to different directions. Previous studies have attributed the different tuning behaviours to functionally different sub-populations [26, 41, 21].

Our model investigates the emergence of these of distinct cell types from the same general network structure based on local differences in recurrent connections combined with asymmetries and biases in the afferent inputs.

Varying the pattern of excitation and inhibition in the direction domain has been previously proposed to simulate these subpopulations in the linear-nonlinear feedforward models (e.g. [43, 41, 31, 21]). However, in these feedforward models, centre-surround interactions (in direction space) can only change the weights of different input directions from V1. These interactions are static and fitted to one type of inputs (e.g. [41] for plaids) and therefore cannot account for all tuning function properties. Only a handful of theoretical studies have proposed that recurrent interactions implementing centre-surround interactions in direction space could help solve the motion integration/segmentation problem but they are restricted to implementing a soft winner-take-all mechanism ([49, 48, 38, 16]). For the first time, our model captures all currently known tuning properties of macaque MT subpopulations when presented with different types of bidirectional motion patterns (e.g. [40, 47, 50, 21]) and condenses several previous hypotheses on the role (and shape) of inhibition in motion integration and segmentation (e.g. [20, 11, 45]). It shows that different sensory tuning functions that are often arbitrarily opposed can be in fact be seen as emergent properties of a single recurrent network where excitation/inhibition balance is dependent on the statistical properties of its inputs.

We identified three key input parameters: the direction separation between input distributions, their width but also their relative strength. These parameters are well known to control global motion perception and in particular whether the two inputs will be integrated, segregated, repulsed or perceived as transparent surfaces (see [4, 5, 6, 27] for reviews). Given the strong links between the different neuronal tuning functions and each of these percepts, our model could be extended with a simple decoding stage to account for human perceptual performance [38]. Many of these perceptual states are seen as depending on opposite (or symmetrical) constraints. Recurrent networks have been already proposed as a solution for solving some aspects of the integration/segmentation problem (e.g. [48, 46, 38, 24] and its associated perceptual multi-stability [37]. Because it can reproduce all MT subpopulations and their dynamics across a generic description of the inputs, the current ring model is a major step toward by establishing the connection between low-level neural dynamics and canonical computations associated with perceptual dynamics

Context dependence of recurrent interactions

An intriguing and controversial property of MT neurons is that, as in many other sensory areas, their direction tuning would depend upon the detailed statistical properties of the inputs ([17, 21, 50]). In a recent comprehensive study, Xiao and Huang [50] claimed that no simple rule can be used to predict how a vector averaging cell identified with a random dot pattern would behave when presented with a plaid pattern with same motion component direction. Only some trends could be identified such as more VA and WTA/SB cells would become pattern and component cells, respectively. However, even such a trend is contradicted in another study that reported the opposite migration pattern in the marmoset monkey [21]. These dynamics in the behaviour could be attributed to the differences in the spatio-temporal inputs (in particular the width of each input) as well as by contextual network modulations in terms of lateral excitation and inhibition strength. Our model provides, for the first time a systemic method to investigate the role of each of these factors.

We reported some of the migration patterns described in macaque area MT [50] and have shown that same network (with fixed connectivity parameters) can dramatically change its behaviour purely by changing from one input to another despite the fact that they have similar

global and component motion directions but different precisions. However, the proportions did not fully agree with the experimental data of [50]. Our results would suggest that the experimentally observed transitions with random dots and plaids are contingent on context-dependent changes for recurrent interactions. For instance, the excitation/inhibition balance might be different from random dot stimuli and for plaids. Further work is needed to unveil the systematic dependence of the recurrent interactions that are needed to predict how MT populations adaptively migrate from one tuning to another. To do so, our qualitative approach would be improved with a systematic fitting of the model parameters to a representative dataset. More important, our study strongly suggests the existence of a context-dependent modulation of the networks connectivity parameters that would depend on the type of stimulus, an explanation that reconciles opposite views on the motion integration/segmentation problem.

A functional consequence of network multi-stability?

Our ring model relies on only four critical parameters in the direction space: the properties of the motion inputs and the centre-surround interactions. Our systematic parameter investigation maps the organisation of parameter regimes where each of the solutions is stable. A bifurcation analysis revealed regions of the parameter space where multiple network states are possible, leading to multi-stability without plasticity [36]. To further characterise the different network behaviours of the network, we ran stochastic simulations with randomised initial conditions to obtain a measure of the strength of the different stable solutions. This allows to relate multi-stability and fluctuations at single-cell levels across trials. We found for instance that when the two inputs are symmetrical, we obtained a lack of specific tuning behaviour and high-variance in single-cell responses. This high variance only introduces some minor fluctuations in the population activity. This result opens the door to several predictions that could be tested empirically. First, it would be important to compare true population tuning with single cell behaviour by contrasting population and unitary recordings. Second, large variability in single cell tuning could be due to network multi-stability. Recently, Ponce-Alvarez and colleagues [32] demonstrated that rate variability and noise correlation in MT neurons can be seen as emergent properties of a stochastic recurrent network for a set of connectivity parameters that overlaps with a single-state solution and multi-stability. However, their model could not explain the rich temporal evolution of neural responses statistics. A further stochastic extension of our ring-model would allow one to render the response variability over the same set of complex stimuli to understand how network multi-stability and neuronal variability are related. It would also call for a re-examination of the large proportion of cells that are unclassified in the different empirical dichotomies that have been used. Third, a small asymmetry in the inputs seems to be critical to stabilise some network solutions and reduce the single-cell variability. Varying the relative contrast or signal-to-noise ratio between the two components would then reduce the variability across trials for MT neurons.

Recurrent models capture slow and fast temporal dynamics of sensory processing

One strength of recurrent network model, when compared with the classical feedforward approach, is the ability to simulate the dynamics of sensory processing. Phenomenological models, often geared toward reproducing psychophysical observations, can capture dynamical characteristics of perceptual competition on slow timescales (generally $> 10s$). These models, either posed in a discrete settings (e.g. [29, 13, 25]) or in a continuous setting [37, 22] have typically focused on dynamical changes in perceived global motion direction or surface motion organisation over

seconds after stimulus onset. We have previously studied both slow and fast, early dynamics of motion integration in a continuous recurrent network featuring direction space, but did not consider neither transparency. Indeed, in all of the previous models, networks operated prominently in a soft winner-take-all mode [37, 13, 38]. The different tuning behaviours in the current ring model would thus allow to investigate not only early temporal dynamics but also population dynamics over slow timescales leading to perceptual shifts between pattern and transparency perceptual interpretations. We have also shown here that the ring model can also render the fast, initial dynamics of motion processing without postulating some specific delays or temporal sensitivities are in previous works [49, 31, 37]. Rather, the time course of inhibition is sufficient to capture the temporal development of MT direction tuning [44, 28] as well as the temporal migration from one computation (e.g., VA) to another (e.g., WTA/SB) [47, 50]. This could further explain similar transitions from initial integration to later segregation, which have been observed in both auditory and visual paradigms at the perceptual [14] and physiological levels [23, 39]. This simple mechanism may account for other temporal aspects of MT pattern/component cells, such as their temporal limits [18] or their responses to triplaids [15].

Conclusion

Recurrent local interactions in the feature domain can reproduce a variety of tuning behaviours that have been reported in the literature. A single ring network model with direction space centre-surround connectivity can capture all of the prototypical tuning curves observed in motion area MT. Interestingly, the attraction strength of different stable solutions and the delayed onset of inhibition, can explain dynamic changes in tuning behaviour observed in physiological experiments. These recurrent interactions can form a bridge between the models of motion integration and models that capture transparency as they eliminate the need for different sub-populations and strong competition (giving only WTA). Further work incorporating spatial interactions are required for more general models to work with a broader range of stimuli.

Methods

Model description We studied the behaviour of direction tuned MT neurons using a continuous ring network model. $u(\theta, t)$ denotes the activity of the neurons tuned to motion direction $\theta \in [-\pi, \pi)$ and the population dynamics is given by the following neural field equation:

$$\frac{du(\theta,t)}{dt} = -u(\theta,t) + \int_{-\pi}^{\pi} J(\theta-\phi)S(\mu u(\phi,t), th)d\phi + k_i * I_{ext}(\theta),$$

where, J is the connectivity kernel defined as a weighted difference of Gaussians $J_{g_e,\sigma_e,g_i,\sigma_i}(\theta) = g_e G(\theta,\sigma_e) - g_i G(\theta,\sigma_i)$, $G(\theta,\sigma)$: Gaussian function, g_e: excitatory strength, σ_e: extent of excitatory surround, g_i: inhibitory strength, σ_i: extent of inhibitory surround. S is a sigmoid function (μ regulates the sigmoidal gain) and I_{ext} is the driving input representative of the motion stimuli.

Representation of visual stimuli using I_{ext}

I_{ext} is defined as a linear combination of gaussian bumps, with each bump describing one component motion direction. The peak width (PW) is defined as the standard deviation of the gaussian bump and renders the inherent uncertainty of the local motion estimation at the V1 stage that feeds the MT layer. The peak separation (PS) describes the difference in the motion direction of the components (see Fig. 1b). These variables allow for a complete description of the two main

classes of uni- and bi-directional motion inputs used in empirical studies: gratings and plaids on one hand and random-dot patterns on the other. It is then possible to compare the model dynamics across different widely used motion inputs.

Numerical study of the model

Exploration of the connectivity space with $\tilde{J}_{\alpha,\beta}$

The impact of main parameters governing the nature of local recurrent interactions, the extent of lateral excitation and strength of lateral inhibition are studied using a family of weighted DoG kernels: $\tilde{J}_{\alpha,\beta}(\theta) = J_{g_{e_\alpha},\sigma_{e_\alpha},g_{i_\alpha}+\beta,\sigma_i}(\theta)$. In particular, we study the case of uniform lateral inhibition and therefore σ_i is fixed to a large value ($\sigma_i = 10\pi$). α is a parameter that smoothly varies the extent of excitatory surround from a narrow (σ_{e_a}) to a broad (σ_{e_b}) bump, depending on a parameter α: $\sigma_{e_\alpha} = \sigma_{e_a} + \alpha\,(\sigma_{e_b} - \sigma_{e_a})$. The other parameters describing the difference of Gaussian functions, g_{e_α} and g_{i_α} are estimated in a closed form with the constraint that, first two Fourier coefficients of $\tilde{J}_{\alpha,0}$, $\widehat{\tilde{J}_{\alpha,0}}[0] = -1$ and $\widehat{\tilde{J}_{\alpha,0}}[1] = 1$, which gives $g_{e_\alpha} = e^{-\frac{\sigma_{e_\alpha}^2}{2}}$ and $g_{i_\alpha} = \frac{1+g_{e_\alpha}}{0.0797}$. β is a free parameter to regulate the strength of lateral inhibition. While considering slow evolution of the inhibition, the inhibition strength g_{i_α} varies with time t as follows: $g_i(t) = g_{i_{low}} + (g_{i_\alpha} + \beta - g_{i_{low}})(1 - \exp\frac{-t}{\tau_I})$.

Parameter regimes supporting transitions

The parametric area supporting a particular transition of interest across different types of inputs (plaids vs. random-dot patterns) is measured by identifying overlapping regimes that support the respective solutions such as VA, WTA or TP. In order to do so, we repeated 100 trials for each input configuration in order to estimate the convergence to each of the solution types. The obtained convergence map was then made binary in order to identify the regimes in which a given solution type is supported. The intersection area of the obtained binary maps would indicate the parameter space supporting the transition of interest. The intersection area relative to the full parameter space was defined is taken as the transition percentage shown in Fig. 6. These computing steps are illustrated in the supplementary Fig. S1.

Population versus Single unit tuning

In physiological experiments, directional selectivity is measured by sequentially presenting stimuli moving in different directions in a randomised manner. Single cell tuning curves are then constructed by averaging responses across trials. Population tuning is often obtained by aggregating tuning across many neurons from either a single subgroup or the complete sample. Population tuning obtained by different means (e.g., Local Field Potentials) is rarely compared to single cells/subpopulation selectivities, albeit with rare exceptions [30]. Such motion direction selectivities are expressed either in terms of the directional preference of MT neurons or in terms of stimulus motion direction, often assuming that these two dimensions are interchangeable [47]. In a ring model, we can construct a joint representation (matrix) of population versus single unit tuning by sequentially assimilating the population tuning to a stimuli at every motion direction within 0 to 360 degrees along the columns allowing us also to sample the single cell preference. As illustrated in Fig. 2b0-b4, each column (or vertical cut) shows the population tuning whereas each row (or horizontal cut) shows the single cell tuning. It is important to notice that assuming recurrent interactions between cells tuned to different directions, the population tuning and single cell selectivities are interchangeable only when the network is operating in a regime with a strong attractor bias.

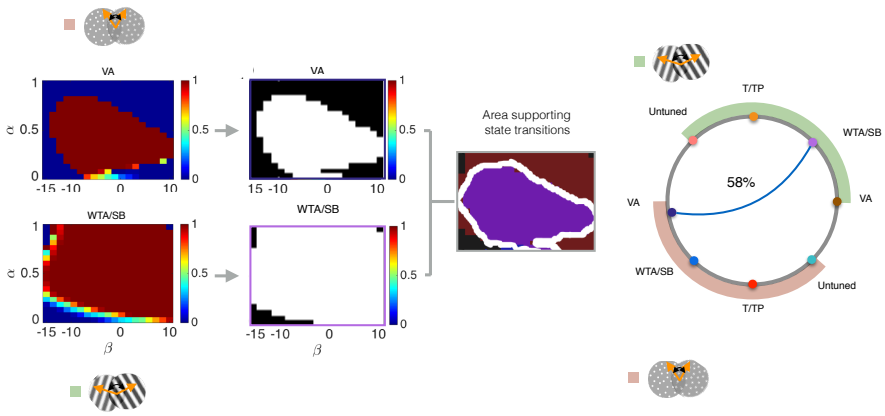

Supplementary Figure 1 (S1): Workflow for computing the percentage of parameter space that supports transitions in the tuning behaviour. For the example inputs bidirectional random dot patterns and plaids, we first computed the parameter space supporting a particular tuning such as WTA/SB and VA, respectively. We then binarised the convergence probability map obtained using 100 repeated trials. In order to measure the space that supports a particular transition, the two binary maps are superimposed to find the area of intersection. The ratio between the intersection and total areas given the frequency of the WTA/SB to/from VA migration reported in the migration diagram on the right-hand column.

Parameter values, initial conditions and numerical computations

The parameters used for the numerical simulations are displayed in Table 1. In case of simulations without noise, standard ode solver, ODE23T was used with absolute tolerance value set to 10^{-12}. For the simulations with noise, the Euler Maruyama method was used. Initial conditions were set to a low level of random activity. In order to carry out numerical continuation and bifurcation analysis, Auto07p package was used, allowing us to track the bifurcation point in one and two-dimensional parameter space. For bifurcation analysis computations were carried out in the absence of noise for a variety of combination of driving input and connectivity kernels. The continuous feature space was discretised into 404 samples.

Acknowledgements

GSM and AIM are supported by a grant from the Agence Nationale de la Recherche (SPEED, ANR-13-SHS2-0006) and by the Centre National de la Recherche Scientifique.The research leading to these results has received funding from the European Union's Seventh Framework Programme (FP7/2007-2013) under grant agreement no. 318723 (MATHEMACS) to PK. JR was partially funded by a Swartz Foundation postdoc grant.

Author contributions statement

All authors designed the study. NVKM and JR elaborated the ring model and ran the simulations. NVKM and GSM wrote the paper.

Description	Parameter	Value
Number of samples in $[-\pi, \pi)$	N	404
Sigmoid threshold	th	3.0
Sigmoid gain	λ	16.0
Input gain	k_i	0.1
Population time constant	τ_p	1.0, 5.0, 10.0
Inhibition time constant	τ_I	30-100
Homotopy variable to regulate excitation width	α	[0,1]
Inhibition offset	β	[-10,15]
Excitation width	$\sigma_{e_\alpha} = \sigma_{e_a} + \alpha\,(\sigma_{e_b} - \sigma_{e_a})$	[11.5°(σ_{e_a}), 60°(σ_{e_b}))
Inhibitory width	σ_i	1800(>> 360)
Excitation strength	g_{e_α}	$e^{-\frac{\sigma_{e_\alpha}^2}{2}}$
Inhibition strength	g_{i_α}	$\frac{1+g_{e_\alpha}}{0.0797}$
Peak Separation	PS	(0, 180]
Peak width	PW	5°-30°

Parameter values used in the numerical studies

Additional information

Some results from this computational study have been presented in international conferences (AREADNE 2016)

References

[1] E.H. Adelson and J.A. Movshon. Phenomenal coherence of moving visual patterns. *Nature*, 300(5892):523–525, 1982.

[2] R. Ben-Yishai, RL Bar-Or, and H. Sompolinsky. Theory of orientation tuning in visual cortex. *Proceedings of the National Academy of Sciences*, 92(9):3844–3848, 1995.

[3] R.T. Born and D.C. Bradley. Structure and function of visual area MT. *Annu. Rev. Neurosci*, 28:157–189, 2005.

[4] O. Braddick. Segmentation versus integration in visual motion processing. *Trends in neurosciences*, 16(7):263–268, 1993.

[5] O. Braddick. Local and global representations of velocity: transparency, opponency, and global direction perception. In *Perception*, volume 26, pages 995–1010. Pion Ltd., 1997.

[6] Oliver Braddick and Ning Qian. *Motion Vision - Computational, neural and ecological constraints*, chapter The organization of global motion and transparency, pages 86–112. Springer-Verlag, 2001.

[7] F. S. Chance, S. B. Nelson, and L. F. Abbott. Complex cells as cortically amplified simple cells. *Nature Neuroscience*, 2:277–282, 1999.

[8] R. Curtu and B. Ermentrout. Pattern formation in a network of excitatory and inhibitory cells with adaptation. *SIAM Journal on Applied Dynamical Systems*, 3:191, 2004.

[9] V.P. Ferrera and H.R. Wilson. Perceived direction of moving two-dimensional patterns. *Vision Research*, 30(2):273–287, 1990.

[10] S. Grossberg, E. Mingolla, and L. Viswanathan. Neural dynamics of motion integration and segmentation within and across apertures. *Vision Research*, 41(19):2521–2553, 2001.

[11] A. Grunwald and M.J. Lankheet. Orthogonal motion after-effect illusion predicted by a model of cortical motion processing. *Nature*, 384(6607):358–360, 1996.

[12] D. Hansel and H. Sompolinsky. *Methods in neuronal modeling: From ions to networks*, chapter 13 Modeling feature selectivity in local cortical circuits, pages 499–567. MIT Press, 1998.

[13] G Huguet, J. Rinzel, and JM. Hupé. Noise and adaptation in multistable perception: noise drives when to switch, adaptation determines percept choice. *Journal of Vision*, 14(3):19, 2014.

[14] J-M Hupé and D Pressnitzer. The initial phase of auditory and visual scene analysis. *Philosophical Transactions of the Royal Society B: Biological Sciences*, 367(1591):942–953, 2012.

[15] Mehrdad Jazayeri, Pascal Wallisch, and Movshon J. Antony. Dynamics of macaque mt cell respnses to grating triplets. *Journal of Neuroscience*, 32(24):8242–8253, 2012.

[16] J. Joukes, T.S. Hartmann, and B. Krekelberg. Motion detection based on recurrent network dynamics. *Frontiers in Systems Neuroscience*, 8(239):1–13, 2014.

[17] F Khawaja and C Pack. Responses of mt neurons to type II plaid stimuli. *Journal of Vision*, 10(7):932–932, August 2010.

[18] Romesh D. Kumbhani, Yasmine El-Shamayleh, and Movshon J. Antony. Temporal and spatial limits of pattern motion sensitivity in macaque mt neurons. *Journal of Neurophysiology*, 113:1977–1988, 2015.

[19] Yuri A Kuznetsov. *Elements of applied bifurcation theory*, volume 112. Springer Science & Business Media, 2013.

[20] W. Marshak and R. Sekuler. Mutual repulsion between moving visual targets. *Science*, 205:1399–1401, 1979.

[21] J. Scott McDonald, Colin W. G. Clifford, Selina S. Solomon, Spencer C. Chen, and Samuel G. Solomon. Integration and segregation of multiple motion signals by neurons in area mt of primate. *Journal of Neurophysiology*, 111(2):369–378, 2014.

[22] Andrew I. Meso, James Rankin, Pierre Kornprobst, and Guillaume S. Masson. The relative contribution of noise and adaptation to competition during tri-stable motion perception. *Journal of Vision*, 16(15):6:1–26, 2016.

[23] C Micheyl, B Tian, RP Carlyon, and JP Rauschecker. Perceptual organization of tone sequences in the auditory cortex of awake macaques. *Neuron*, 48(1):139–148, 2005.

[24] Kenneth D Miller. Canonical computations of cerebral cortex. *Current Opinion in Neurobiology*, 37:75–84, 2016.

[25] R. Moreno-Bote, J. Rinzel, and N. Rubin. Noise-induced alternations in an attractor network model of perceptual bistability. *Journal of Neurophysiology*, 98(3):1125–1139, 2007.

[26] J.A. Movshon, E.H. Adelson, M.S. Gizzi, and W.T. Newsome. The analysis of visual moving patterns. *Pattern recognition mechanisms*, pages 117–151, 1985.

[27] Shin'ya Nishida. Advacement of motion psychophysics: review 2001-2010. *Journal of Vision*, 11(5):11, 1–53, 2011.

[28] C.C. Pack and R.T. Born. Temporal dynamics of a neural solution to the aperture problem in visual area MT of macaque brain. *Nature*, 409:1040–1042, February 2001.

[29] Alexander Pastukhov, Pedro E. Garcia-Rodriguez, Joachim Haenicke, Antoni Guillamon, Gustavo Deco, and Joachim Braun. Multi-stable perception balances stability and sensitivity. *Frontiers in computational neuroscience*, 7(17):1–18, 2013.

[30] Carlyn A. Patterson, Stephanie C. Wissig, and Adam Kohn. Adaptation disrupts motion integration in the primate dorsal stream. *Neuron*, 81(3):674–686, 2014.

[31] J.A. Perrone and R.J. Krauzlis. Spatial integration by MT pattern neurons: a closer look at pattern-to-component effects and the role of speed tuning. *Journal of Vision*, 8(9):1–14, 2008.

[32] Adrián Ponce-Alvarez, Alexander Thiele, Thomas D. Albright, Gene R. Stoner, and Gustavo Deco. Stimulus-dependent variability and noise correlations in cortical mt neurons. *Proceedings of the National Academy of Sciences*, 110(32):13162–13167, 2013.

[33] Nick J. Priebe, S.G. Lisberger, and J. Anthony Movshon. Tuning for spatiotemporal frequency and speed in directionally selective neurons of macaque striate cortex. *Journal of Neuroscience*, 26(11):2941–2950, 2006.

[34] N.J. Priebe, C.R. Cassanello, and S.G. Lisberger. The neural representation of speed in macaque area mt. *Journal of Neuroscience*, 23(13):5650–5661, 2003.

[35] N. Qian, R.A. Andersen, and E.H. Adelson. Transparent motion perception as detection of unbalanced motion signals. III. Modeling. *The journal of Neuroscience*, 14(12):7381–7392, December 1994.

[36] M.M. Quiroga, A.P. Morris, and B. Krekelberg. Adaptation without plasticity. *Cell Reports*, 17:58–68, 2016.

[37] James Rankin, Andrew I. Meso, Guillaume S. Masson, Olivier Faugeras, and Pierre Kornprobst. Bifurcation study of a neural fields competition model with an application to perceptual switching in motion integration. *Journal of Computational Neuroscience*, 36(2):193–213, 2014.

[38] Florian Raudies, Ennio Mingolla, and Heiko Neumann. A model of motion transparency processing with local center-surround interactions and feedback. *Neural Computation*, 23(11):2868–2914, 2011.

[39] GH Recanzone and RH Wurtz. Shift in smooth pursuit initiation and MT and MST neuronal activity under different stimulus conditions. *Journal of Neurophysiology*, 82(4):1710–1727, 1999.

[40] H.R. Rodman and T.D. Albright. Single-unit analysis of pattern-motion selective properties in the middle temporal visual area (MT). *Experimental Brain Research*, 75:53—64, 1989.

[41] N.C. Rust, V. Mante, E.P. Simoncelli, and J.A. Movshon. How MT cells analyze the motion of visual patterns. *Nature Neuroscience*, 9:1421–1431, 2006.

[42] R. Shapley, M. Hawken, and D.L. Ringach. Dynamics of orientation selectivity in the primary visual cortex and the importance of cortical inhibition. *Neuron*, 38(5):689–699, 2003.

[43] E.P. Simoncelli and D.J. Heeger. A model of neuronal responses in visual area MT. *Vision Research*, 38:743–761, 1998.

[44] M. Smith, N. Majaj, and A. Movshon. Dynamics of motion signaling by neurons in macaque area MT. *Nature Neuroscience*, 8(2):220–228, February 2005.

[45] Gene R. Stoner and Thomas D. Albright. Neural correlates of perceptual motion coherence. *Nature*, 358:412–414, 1992.

[46] Emilien Tlapale, Guillaume S. Masson, and Pierre Kornprobst. Modelling the dynamics of motion integration with a new luminance-based diffusion mechanism. *Vision Research*, 50:1676–1692, 2010.

[47] S. Treue, K. Hol, and H.J. Rauber. Seeing multiple directions of motion – physiology and psychophysics. *Nature Neuroscience*, 3(3):270–276, 2000.

[48] Ruye Wang. A network model of motion processing in area mt of primates. *Journal of Computational Neuroscience*, 4(4):287–308, 1997.

[49] H.R. Wilson, V.P. Ferrera, and C. Yo. A psychophysically motivated model for two-dimensional motion perception. *Visual Neuroscience*, 9(1):79–97, July 1992.

[50] Jianbo Xiao and Xin Huang. Distributed and Dynamic Neural Encoding of Multiple Motion Directions of Transparently Moving Stimuli in Cortical Area MT. *The Journal of Neuroscience*, 35(49):16180–16198, December 2015.

[51] C. Yo and H.R. Wilson. Perceived direction of moving two-dimensional patterns depends on duration, contrast and eccentricity. *Vision Research*, 32(1):135–47, 1992.

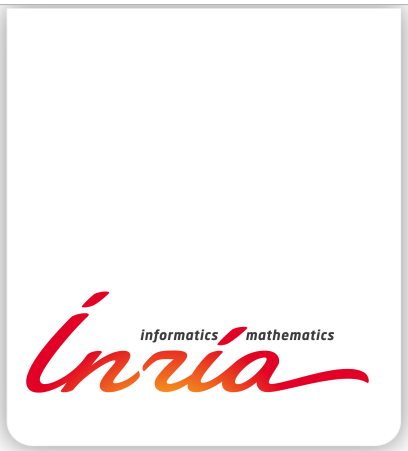

RESEARCH CENTRE
SOPHIA ANTIPOLIS – MÉDITERRANÉE

2004 route des Lucioles - BP 93
06902 Sophia Antipolis Cedex

Publisher
Inria
Domaine de Voluceau - Rocquencourt
BP 105 - 78153 Le Chesnay Cedex
inria.fr

ISSN 0249-6399